Tellus (2004), 56A, 342–361
Printed in UK. All rights reserved

TELLUS

Transient response of the Atlantic Meridional Overturning Circulation to enhanced freshwater input to the Nordic Seas–Arctic Ocean in the Bergen Climate Model

By ODD HELGE OTTERÅ[1,2]*, HELGE DRANGE[1,2,3,4], MATS BENTSEN[1,2], NILS GUNNAR KVAMSTØ[2,3] and DABANG JIANG[4], [1]*Nansen Environmental and Remote Sensing Center, Edv. Griegsvei 3A, 5059 Bergen, Norway;* [2]*Bjerknes Centre for Climate Research, Allégt. 55, 5007 Bergen, Norway;* [3]*Geophysical Institute, University of Bergen, Allégt. 70, 5007 Bergen, Norway;* [4]*Nansen-Zhu International Research Centre, Beijing 100029, China*

(Manuscript received 6 May 2003; in final form 29 January 2004)

ABSTRACT

The transient response of the climate system to anomalously large freshwater input to the high latitude seas is examined using the newly developed Bergen Climate Model. A 150-yr twin-experiment has been carried out, consisting of a control and a freshwater integration. In the freshwater integration, the freshwater input to the Arctic Ocean and the Nordic Seas is artificially increased by a factor of 3, or to levels comparable to those found during the last deglaciation. The obtained response shows a reduced maximum strength of the Atlantic Meridional Overturning Circulation (AMOC) over the first 50 yr of about 6 Sv (1 Sv $=10^6$ m^3 s^{-1}), followed by a gradual recovery to a level comparable to the control integration at the end of the period.

The weakened AMOC in the freshwater integration is caused by reduced deep-water formation rates in the North Atlantic subpolar gyre and in the Nordic Seas, and by a reduced southward flow of intermediate water masses through the Fram Strait. The recovery of the AMOC is caused by an increased basin-scale upwelling in the Atlantic Ocean of about 1 Sv, northward transport of saline waters originating from the western tropical North Atlantic, and a surface wind field maintaining the inflow of Atlantic Water to the Nordic Seas between the Faroes and Scotland.

Associated with the build-up of more saline waters in the western tropical North Atlantic, a warming of ∼0.6 °C over the uppermost 1000 m of the water column is obtained in this region. This finding is consistent with paleo records during the last deglaciation showing that the tropics warmed when the high latitudes cooled in periods with reduced AMOC.

Furthermore, the results support the presence of a coupled North-Atlantic-Oscillation-like atmosphere–sea-ice–ocean response mode triggered by the anomalous freshwater input. Throughout most of the freshwater integration, the atmospheric circulation is characterized by anomalously low sea level pressure in the Nordic Seas and anomalously high sea level pressure over Spain. This forces the North Atlantic Drift to follow a more easterly path in the freshwater integration than in the control integration, giving an asymmetric sea surface temperature response in the northern North Atlantic, and thereby maintaining the properties of the Atlantic Water entering the Nordic Seas between the Faroes and Scotland throughout the freshwater integration.

1. Introduction

A key challenge in climate research addresses the stability of the large-scale Meridional Overturning Circulation (MOC) of the ocean. This is partly caused by the large amount of heat transported with the MOC, and partly caused by the decadal-to-century time-scale memory associated with natural or forced variations in the MOC. For the present-day ocean circulation, significant changes to climate would follow from a collapse of the MOC (e.g. Manabe and Stouffer, 1997; Vellinga et al., 2002).

Evidence from paleo records indicates that the Earth underwent large and rapid climate changes during the last glacial and post-glacial periods. The isotopic (δ^{18}O) temperature records from the Greenland ice cores have revealed a series of rapid climate changes between 20 000 and 100 000 yr before present

*Corresponding author.
e-mail: oddho@nersc.no

(BP). The origin of the abrupt changes is heavily discussed, but a number of studies suggest that the MOC plays an active and important role in these rapid climate transitions (Broecker et al., 1985; Broecker, 1997; Ganopolski and Rahmstorf, 2001).

Numerous modelling studies have demonstrated that the Atlantic surface freshwater balance is a key control parameter for the strength and variability of the MOC. It is a common finding from simplified and coupled atmosphere–sea-ice–ocean models that the strength of the MOC reduces if there is a net flux of freshwater added to the high northern latitudes (Manabe and Stouffer, 1997; Schiller et al., 1997; Rind et al., 2001; Vellinga et al., 2002). This response is often described in terms of Stommel's classical feedback (Stommel, 1961): a high latitude input of freshwater will decrease the overturning and a more sluggish surface flow is exposed longer to the freshwater forcing. Another destabilizing feedback on the MOC is related to the atmospheric transport of moisture (Marotzke and Stone, 1995): a weaker MOC cools the high latitudes and thus increases meridional temperature gradients. This leads to a stronger meridional circulation in the atmosphere and a stronger meridional moisture flux. The stronger import of moisture to the high latitudes decreases the sea surface salinity (SSS) and thus enhances the reduction of the MOC.

In the coupled atmosphere–ocean model of Schiller et al. (1997), a massive discharge of freshwater at the surface of the north-west Atlantic Ocean led to a shutdown of the production of North Atlantic Deep Water. However, upon termination of the freshwater forcing, the AMOC reintensified and regained its original intensity after a few centuries. The study of Schiller et al. (1997) points to a cooling of the high latitudes and changes in the wind-driven circulation as mechanisms responsible for the recovery of the AMOC. Similarly, Vellinga et al. (2002) found a recovery of the AMOC in about 120 yr after the AMOC initially had been suppressed by a strong salinity perturbation in the northern North Atlantic. A key mechanism in their simulation was the creation and subsequent northward advection of positive salinity anomalies from the western tropical North Atlantic (WTNA). On the other hand, in the model of Rind et al. (2001) the AMOC did not recover after it had been shut down through anomalous freshwater input from the St Lawrence river.

The role of freshwater forcing at high latitudes is also important in a future perspective. Most greenhouse gas simulations yield strong perturbations of the hydrological cycle with enhanced freshwater flux to high northern latitudes (Räisänen, 2001). However, the actual response of the AMOC varies between the models, with some indicating a weakening of about 50%, while others show essentially no change (Cubasch et al., 2001). There is thus a large degree of uncertainty regarding the stability of the present-day AMOC and, more specially, its sensitivity to anomalous high northern freshwater forcing. A better understanding of the physical processes and feedbacks that control the stability of the AMOC, and how these feedbacks work, is therefore clearly needed.

In the present study, the transient effect of increased freshwater fluxes to the Nordic Seas and the Arctic Oceans is examined using the newly developed Bergen Climate Model (BCM), a fully coupled ocean–sea-ice–atmosphere model (Furevik et al., 2003). The main results of the freshwater experiment have already been presented in Otterå et al. (2003). It was here found that the modelled AMOC was relatively robust to high latitude freshwater forcing, and several stabilizing mechanisms for the AMOC were identified. In the present study, these proposed stabilizing mechanisms are explored in more detail.

The performed model experiment is not intended to give an exact picture of any particular geological event (e.g. the Younger Dryas period), as the solar insolation, vegetation, topography and orography, composition of the atmospheric greenhouse gases, aerosol particles, etc., are all given present values. However, the results might be applicable in explaining and interpreting possible processes and feedback mechanisms of relevance for past as well as possibly future climate changes.

The paper is organized as follows. The model and the set-up of the freshwater experiment are described in Section 2. In Section 3, the model results are presented. The different feedback mechanisms and comparisons to past climate changes and other model studies are discussed in Section 4, and some final comments are given in Section 5.

2. Model description and set-up of the experiment

The atmosphere component is the spectral atmospheric general circulation model ARPEGE/IFS from Météo-France (Déqué et al., 1994). In the present study, ARPEGE/IFS is run with a truncation at wavenumber 63 (T_L63), and a time-step of 1800 s. The grid point calculations are carried out with a grid of horizontal resolution of about 2.8°. A total of 31 vertical levels are employed, ranging from the surface to 0.01 hPa (20 layers in the troposphere). The physical parametrization is divided into several explicit schemes, which each calculates the flux of mass, energy and/or momentum due to a specific physical process. Different from the model description in Déqué et al. (1994), the version used in the BCM contains a convective gravity drag parametrization (Bossuet et al., 1998), a new snow scheme (Douville et al., 1995), increased orographic drag (Lott, 1999) and modifications in deep convection and soil vegetation schemes. Further details of the ARPEGE model applied in this study are provided in Furevik et al. (2003).

The oceanic component of the BCM is the Miami Isopycnic Coordinate Ocean Model (MICOM) described in Bleck et al. (1992). The horizontal grid has 2.4° resolution along the equator with one pole over Siberia and the other over the South Pole, and the primitive equations are discretized on an Arakawa-C grid.

The ocean grid is mostly regular except for a band along the equator, where the meridional spacing is gradually increased to 0.8° to better resolve equatorial-confined dynamics. The version used in this study has 24 layers in the vertical; a mixed layer (ML) with a temporal and spatial varying density, and 23 isopycnal layers below with potential densities ranging from $\sigma_\theta = 24.12$ to $\sigma_\theta = 28.10$.

The vertically homogeneous ML utilizes the Gaspar et al. (1990) bulk parametrization for the dissipation of turbulent energy, and has temperature, salinity and layer thickness as prognostic variables. In the isopycnic layers, temperature is treated as a prognostic variable while salinity is diagnosed from a simplified equation of state (Friedrich and Levitus, 1972). This differs from the original formulation of MICOM where salinity was chosen as a prognostic variable, and is motivated by the fact that the diagnosed temperature is very sensitive to small variations in salinity in cold water and freshwater. In order to avoid possible problems at high latitudes, temperature was therefore chosen as a prognostic variable.

In the present version of the BCM, dynamic and thermodynamic sea-ice modules are integrated parts of the ocean model. The thermodynamic module incorporates freezing and melting of sea-ice and snow-covered sea-ice, and is based on the thermodynamics of Drange and Simonsen (1996). The dynamic part follows the viscous-plastic rheology of Hibler (1979), with further modifications by Harder (1996).

The atmosphere and the ocean models are coupled using the Ocean Atmosphere Sea-Ice Soil (OASIS) coupler (Terray et al., 1995). In the BCM, the two models exchange data once every day. Fluxes of heat, mass (freshwater) and momentum (wind stress) are taken as forcing for the ocean model. In addition, the atmospheric model passes surface temperature and albedo to OASIS, which are used to modify the heat fluxes by a subgrid method described in Furevik et al. (2003). The sea surface temperature (SST), the sea-ice cover and the sea surface and sea-ice/snow albedos serve as lower boundary conditions for the atmosphere model. For further details on the coupling procedure, see Furevik et al. (2003).

An automatic procedure, using the Total Runoff Integrating Pathways (TRIP) data set (Oki and Sud, 1998), has been implemented to assign each land point in the atmosphere model to discharge points along the coast in the ocean model. This information is used by OASIS to exchange runoff directly with coastal ocean grid cells. Furthermore, a scheme that smoothes the freshwater discharge to the ocean in a conservative manner is included (Furevik et al., 2003).

The basis for the experiment is the modern state as simulated by the 300-yr control (CTRL) run with the BCM (Furevik et al., 2003). The freshwater experiment (FW) is carried out by perturbing the modelled state in year 100 of CTRL with a threefold increase in the river runoff to the high northern latitude seas, and then running the model for another 150 yr. The anomalous freshwater input is continuously and instantaneously added to the coastal regions in the Nordic Seas and the Arctic Ocean during the integration (Fig. 1).

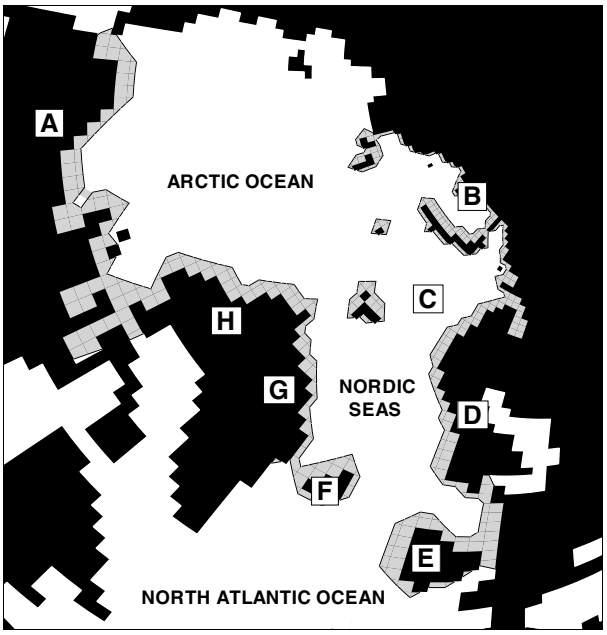

Fig 1. The major meltwater discharge areas in the Nordic Seas and the Arctic Oceans during the last deglaciaton according to Simonsen (1996): A, Arctic Ocean; B, Kara Sea; C, Barents Sea; D, Western Norway; E, British Islands; F, Iceland; G, East Greenland; H, North Greenland. The shaded regions represent the model grid cells where the river runoff is increased in the freshwater experiment.

In CTRL, the river runoff is about 0.1 Sv, or comparable to the estimates given by Aagaard and Carmack (1989) for the present-day climate system. In FW, the river runoff is increased to 0.4 Sv, which represents a perturbation of the system similar to the simulated increase in the total freshwater input poleward of 50°N obtained at a quadrupling of the pre-industrial CO_2 level (Manabe and Stouffer, 1994). The freshwater flux is also believed to be consistent with the meltwater entering the high northern oceans during the last deglaciation (Simonsen, 1996). Both comparisons illustrate that the applied freshwater flux is strong.

It is important to note that the increased freshwater flux has been artificially added to the system in contrast to a full climate-change scenario with an internally consistent hydrological cycle. The performed integration should therefore be viewed as a sensitivity experiment only. Obviously, 150 yr is too short to describe any long-term changes in the climate system. A realization of the decadal to multidecadal transient response is, however, captured over such an integration period.

Finally, to avoid drift from climatological SST and SSS fields, the heat and freshwater fluxes are adjusted based on a time-invariant flux-correction derived from the spin-up of the model (Furevik et al., 2003). For the subpolar region (48°N–65°N) and

the subtropical/tropical Atlantic (15°S–15°N), the salt flux adjustment corresponds to a net freshwater supply of about 0.2 and 1 Sv, respectively. The freshwater perturbation in FW is therefore comparable to the applied salt flux adjustment for the subpolar region.

3. Results

3.1. AMOC and deep water formation responses

A common diagnostics for the strength of the large-scale ocean circulation in the Atlantic is the maximum strength of the AMOC. In Fig. 2a, a 5-yr running mean of the maximum value of the AMOC is provided. In CTRL, the AMOC exhibits decadal variations of a few Sv around the mean value of about 18 Sv. In FW, the major change in the maximum AMOC takes place over the first 50 yr, with suppressed decadal variability and a drop in the strength of the AMOC of up to about 6 Sv. There is a gradual and fairly constant recovery of the AMOC over the following 100 yr, reaching a value of about 16 Sv in year 150. The decadal variability characteristics are fairly similar between the two runs between year 50 and 150. The changes in the northward heat transport across 24°N are very similar to the changes in the AMOC: during the first 50 yr, the northward heat transport is reduced by about 0.2 PW. However, as the AMOC recovers during the following 100 yr, the heat transport increases by about 0.1 PW.

In the study of Bentsen et al. (2004), it was found that the decadal-scale variability of the AMOC in the BCM is closely linked to the variability in the convective winter mixing, and consequently to the formation of intermediate to deep water masses, in the North Atlantic subpolar gyre. The convective mixing regions in the BCM are located in the Labrador, the Irminger and the Nordic Seas as depicted in Fig. 3. Time series of the mixing

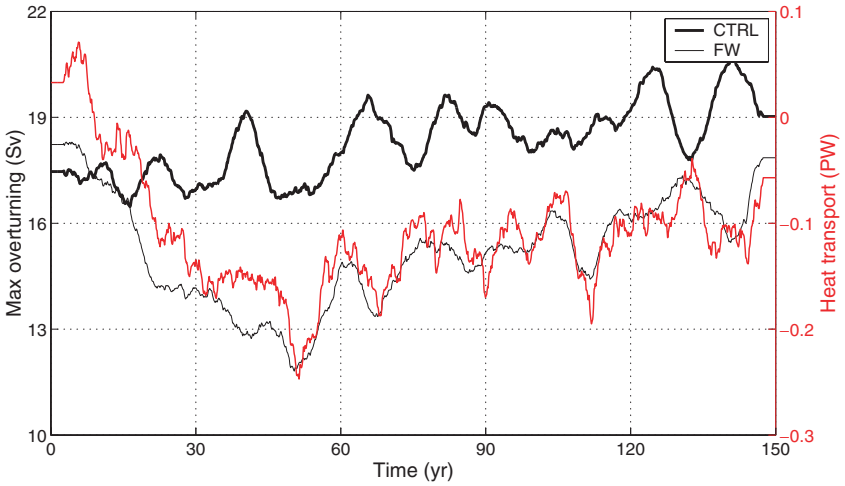

(a)

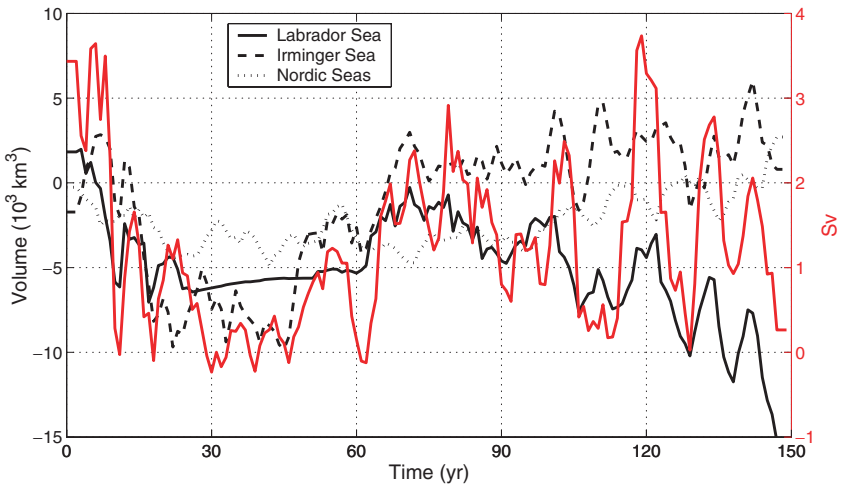

(b)

Fig 2. Time series of (a) the maximum AMOC (Sv) in FW and CTRL and the difference (FW–CTRL) of the mean northward heat transport (PW) across 24°N (red curve), and (b) the difference (FW–CTRL) of the mean volume (km^3) of the ML water extending below 500 m in the Labrador Sea (solid line), the Irminger Sea (dashed line) and the Nordic Seas (dotted line) in March. In addition, the amount of water (Sv) that mixes below the 27.63 isopycnal in March in the subpolar region (50°N–63°N) is shown in red. All time series have been smoothed using a 5-yr running mean filter. The northward heat transport in (a) is defined as the heat carried with the northward flow and relative to 0°C. The flat ends of the curves, as well as the offset between FW and CTRL at year 0, are due to the applied filtering scheme.

Fig 3. The shading shows the areas in CTRL and FW where the March ML depth exceeds 1500 m at least once during the 150-yr integration.

intensity averaged over the mixing regions in March, the month with strongest mixing, are provided in Fig. 2b. The changes are, in general, most profound for the subpolar region (Labrador and Irminger Seas). Here the deep mixing decreases over the first 40 yr of the integration, followed by a fairly quick recovery over the subsequent 20–30 yr. A gradual reduction in the mixing intensity in the Labrador Sea during the last 60–70 yr of FW can also be noted, whereas the deep mixing in the Irminger Sea actually increases. The variations in the mixing in the Nordic Seas are generally smaller compared to those in the subpolar gyre.

In order to give a rough estimate of the change in the intermediate and deep-water mass formation in the subpolar region, the volume rate of water masses that mixes below the 27.63 isopycnal in March is calculated for FW (Fig. 2b, red curve). The result shows an approximate reduction in excess of 3 Sv over the first 50 yr and a subsequent recovery of about 1.5 Sv over the following 100 yr.

The difference between the AMOC stream functions in FW and CTRL is displayed in Fig. 4. For years 21–40, a reduction in the strength of the AMOC in FW of 4–5 Sv is found between the equator and 50°N at depths between 800 and 4000 m, whereas the overturning at 1000 m depth is reduced by 2–3 Sv (Fig. 4a). A recovery of the AMOC is clearly seen between 20°N and 55°N at depths between 1000 and 2000 m at the end of the integration (Fig. 4b).

3.2. Salinity, temperature and sea-ice responses

Figure 5a shows the SSS changes in FW at the end of the integration period. The strongest freshening is found in the vicinity of the main freshwater discharge areas in the Nordic Seas and the Arctic Ocean. In the Nordic Seas, a freshwater plume is carried poleward by the Norwegian Atlantic Current. A relative small change (less than 0.1 psu) is found in the central to western part of the Nordic Seas.

In the Arctic Ocean, the freshwater input leads to a profound freshening of the surface layer. By the end of the period, the salinity over the entire Arctic Ocean is reduced by about 0.8 psu. The freshwater flowing southward through the Canadian Archipelago is clearly seen as a freshwater lens covering the Atlantic Ocean west of the mid-Atlantic ridge and poleward of 40°N.

Outside the North Atlantic–Arctic region, positive SSS anomalies are found in the Atlantic between 45 and 30°S and in the central Indian Ocean towards the end of the integration. These SSS anomalies are caused by increased SSTs (see below) and consequently enhanced evaporation in the South Atlantic, and reduced precipitation in the central Indian Ocean (not shown).

The spatial distribution of the SST anomalies for the last 40 yr is provided in Fig. 5b. The most noticeable feature is a distinct asymmetric response in the northern North Atlantic, with a strong cooling (in excess of 2°C) in the subpolar gyre and a slight warming in the eastern part of the northern North Atlantic. In the eastern part of the Barents Sea, a cooling in excess of 1°C is found. In the Nordic Seas, positive SST anomalies are obtained, with the strongest warming taking place south of the Fram Strait.

Another feature in FW is the gradual changes in the vertical distributions of temperature and salinity found in the tropical Atlantic (Figs. 6 and 7). Towards the end of the integration, positive salinity anomalies, even when zonally averaged, are found over the upper 1000 m of the water column from about 40°S to about 20°N (Fig. 6). In addition, negative salt anomalies are seen to propagate southward along with the North Atlantic Deep Water at a depth of 2000–3000 m (e.g. Gao et al., 2003). The evolution of the temperature of the upper 1000 m of the water column in the Guyana Current (Fig. 7) shows a subsurface warming of about 0.2°C (0.4°C) in year 30 (70). The subsurface warming persists throughout most of the integration period. Furthermore, it should be noted that the cold anomaly at 1500–2000 m originates from the deep mixing in the Irminger Sea over the last part of the integration (Fig. 2b).

The temporal and spatial changes in the sea-ice distribution in FW are shown in Fig. 8. In the Labrador and Barents Seas, a strong increase in the sea-ice area is found early in the period, with increases of about 150 000 and 250 000 km^2, respectively. Towards the end of the integration there is a gradual reduction and subsequent stabilization of the sea-ice area in the Barents Sea, whereas a more gradual, long-term change in the sea-ice area is found in the Labrador Sea.

3.3. Atmospheric responses

The changes in the annual mean surface air temperature are shown in Fig. 9. There is a general cooling at the high

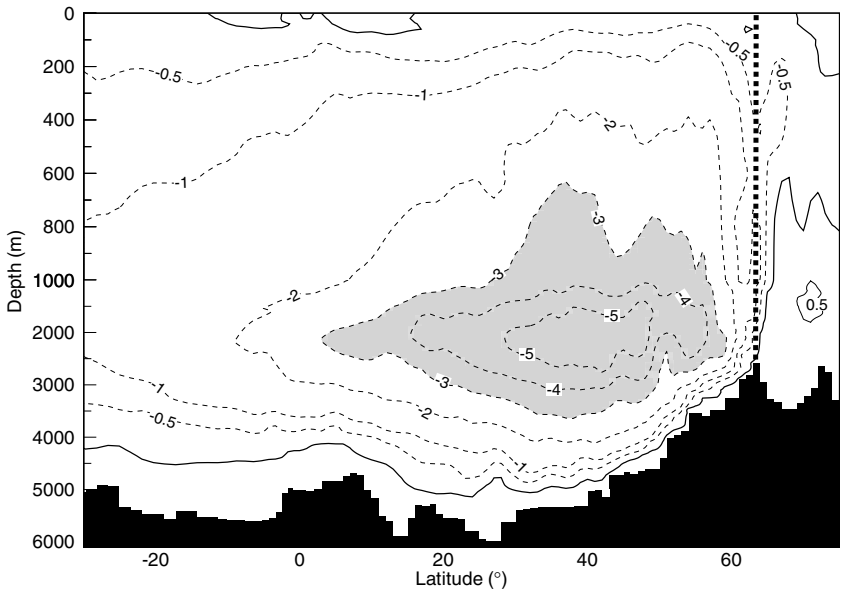

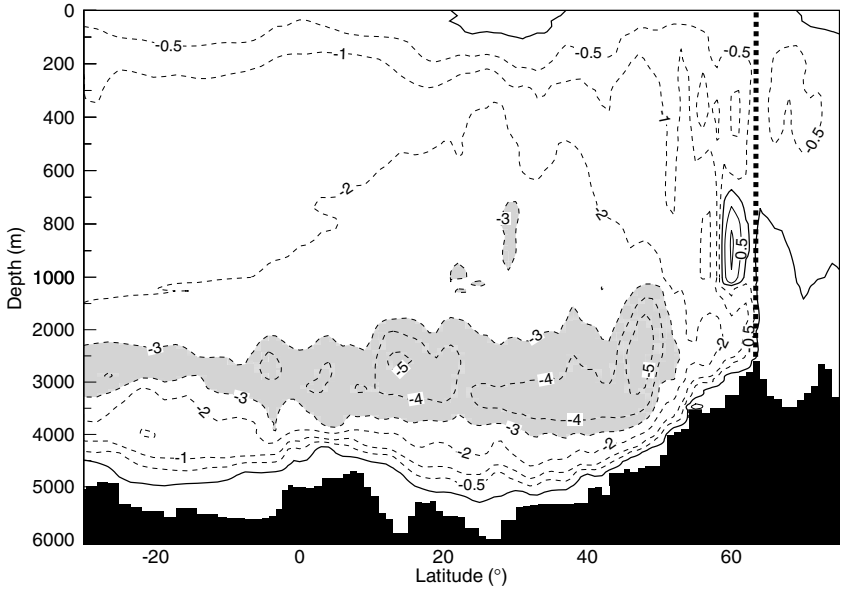

Fig 4. The difference (FW–CTRL) in the AMOC stream function as function of depth. Mean values are provided for years 21–40 (a), and years 131–150 (b). Contour interval is 1 Sv. In addition the 0.5 Sv contour isoline is shown. The shading indicates differences greater than 3 Sv. The vertical line at 63°N indicates the location of the Greenland–Scotland ridge.

northern latitudes during the whole period, with the strongest signal found in the western part of the northern North Atlantic (-2°C) and in the eastern Barents Sea (-1°C or more). Furthermore, there is a cooling of between 0.5 and 1°C over most of the North American continent, and between 1 and 2°C over the central and north Eurasian continent. In the western part of the Nordic Seas, a slight warming can be seen in the early period (Fig. 9a). For the last 40 yr, the warming in the Nordic Seas has increased in strength and has spread into the Arctic Ocean (Fig. 9b).

The changes in the atmospheric freshwater and heat fluxes are provided in Fig. 10. The net heat fluxes towards the end of the integration (Fig. 10a) show a negative heat flux anomaly of >15 W m^{-2} in the central North Atlantic and south of the Fram Strait (meaning an enhanced heat flux from the ocean to the atmosphere), and a positive anomaly in the north-western part of the North Atlantic (>40 W m^{-2}) and in the eastern part of the Barents Sea (about 20 W m^{-2}). The positive heat flux anomalies in the Labrador and Barents Seas (Fig. 10a) are closely related to the advancing sea-ice in these regions in winter (Fig. 8).

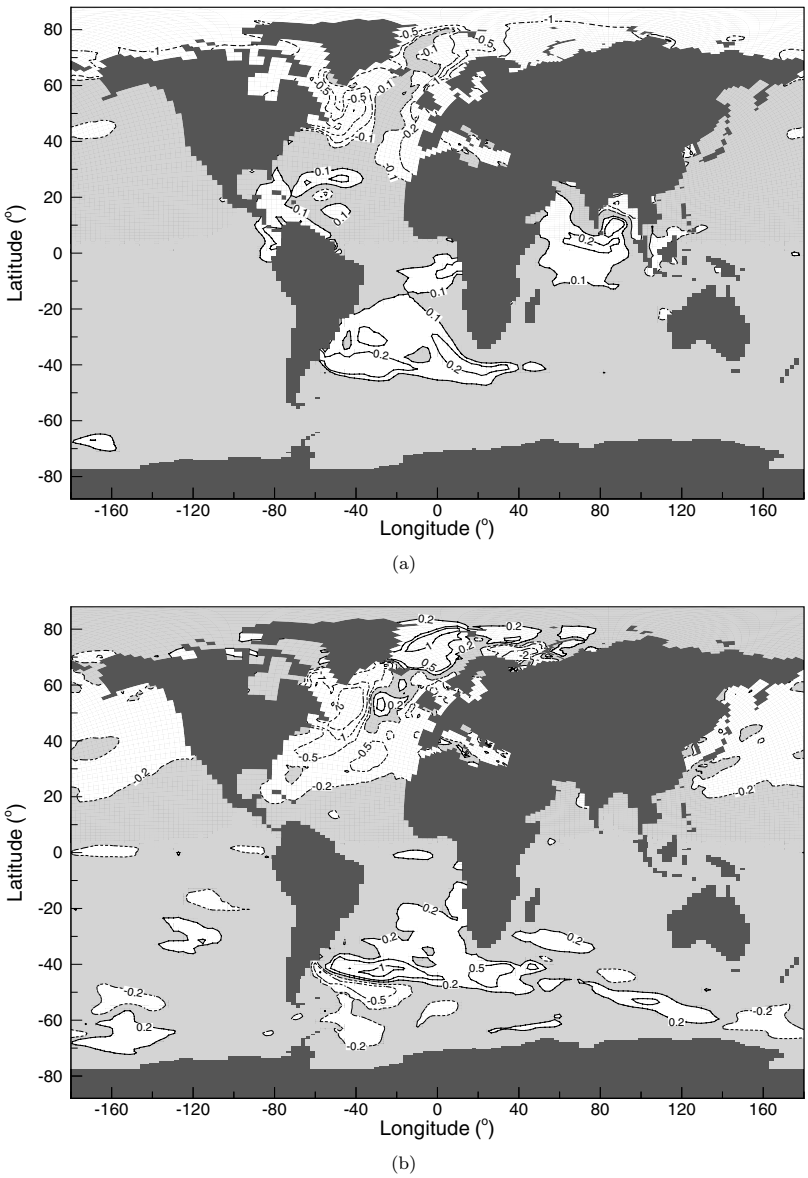

Fig 5. (a) Difference (FW–CTRL) in SSS (psu) for the last 40 yr of the integration. Contour isolines are 0.1, 0.2, 0.5 and 1 psu. (b) As in (a), but for SST (°C). Contour isolines are 0.2, 0.5, 1 and 2°C.

The changes in the atmospheric freshwater fluxes (Fig. 10b) resemble those found for the heat fluxes. In the northern North Atlantic there is an asymmetric pattern, with positive freshwater flux anomalies (net flux of freshwater directed from the atmosphere to the ocean) in the western part and negative anomalies in the central part. Furthermore, negative freshwater flux anomalies are found in the Nordic Seas south of the Fram Strait, tending to increase the SSS in this region. In the equatorial Atlantic, a distinct dipole pattern is found in the atmospheric freshwater fluxes (Fig. 10b), reflecting a south-eastward shift in the position of the intertropical convergence zone (ITCZ) and the precipitation maximum associated with it (not shown).

The natural variability of the present-day North Atlantic–Arctic climate system is highly governed by anomalies in the spatial–temporal distribution of the atmospheric mass in the region (Visbeck et al., 2003). The winter sea level pressure (SLP) difference between FW and the mean state for CTRL for years 11–50 (Fig. 11a) shows increased SLP over the Azores and reduced SLP in the Nordic Seas, very similar to a positive North Atlantic Oscillation (NAO) state. The changes in the wind field show enhanced westerlies in the North Atlantic, and enhanced northerlies in the western part of the Nordic Seas. In the Arctic region, high pressure develops over the Kara Sea, leading to north-westward flow anomalies across the Barents Sea.

For the rest of the integration period, the low pressure over the Nordic Seas is reduced and moved slightly southwestwards (Fig. 11b). Furthermore, a relatively strong low-pressure anomaly can be seen to develop over Russia. The

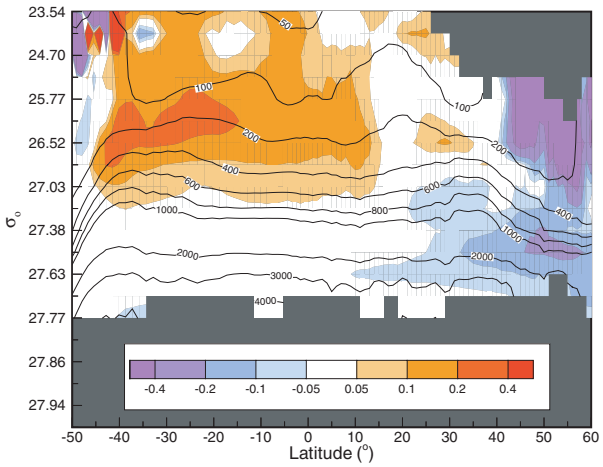

Fig 6. Zonally averaged anomalies (FW–CTRL) of the annual mean salinity (psu) as a function of potential density (σ_0) and latitude for years 131–150. The depths (m) of the isopycnals are imposed as contour lines.

high-pressure anomaly over the Kara and Barents Seas, with an accompanying south-easterly wind anomaly, persists throughout the period. In the northern North Atlantic, the high-pressure anomaly over the Azores is now located over Spain. Furthermore, a local positive SLP anomaly can be seen in the southern part of the Irminger Sea. The net result of these changes is a south-westerly wind anomaly in the eastern North Atlantic directed towards the eastern part of the Greenland–Scotland ridge. Finally, a tendency towards lower pressure in the subtropical Atlantic can be seen, with northerly wind anomalies across the equator.

3.4. *Ocean transport response*

The changes in the ocean transports in and out of the Arctic Mediterranean (e.g. the Nordic Seas, the Arctic Ocean, and the Barents and Kara Seas) can be quantified by examining the changes in the volume transports in the region. Across the

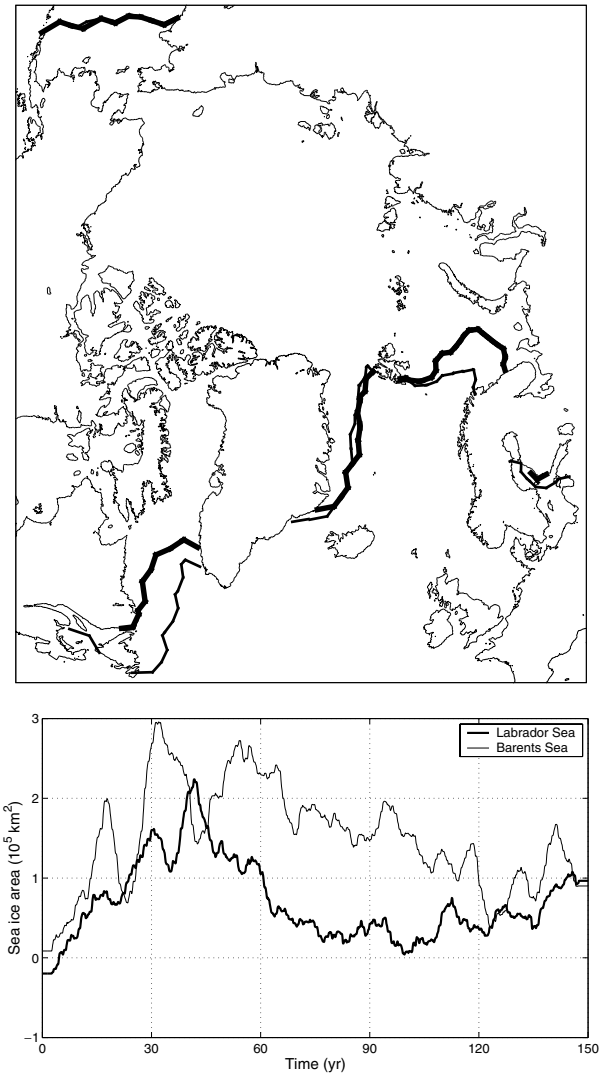

Fig 8. Spatial and temporal changes in the average sea-ice extent. The upper panel shows the sea-ice margin in CTRL (thick line) and FW (thin line) in March for years 11–50. The lower panel shows the temporal evolution of the sea-ice area in the Barents Sea (thin line) and the Labrador Sea (thick line).

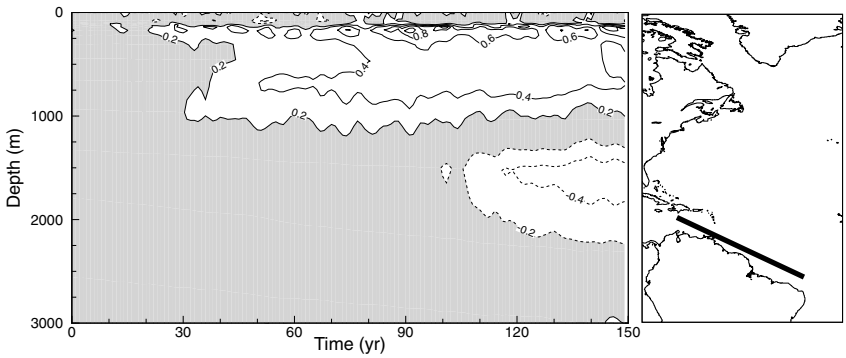

Fig 7. Temporal evolution of the temperature anomaly (°C) averaged over the Guyana Current section. The section is shown in the right-hand side of the panel.

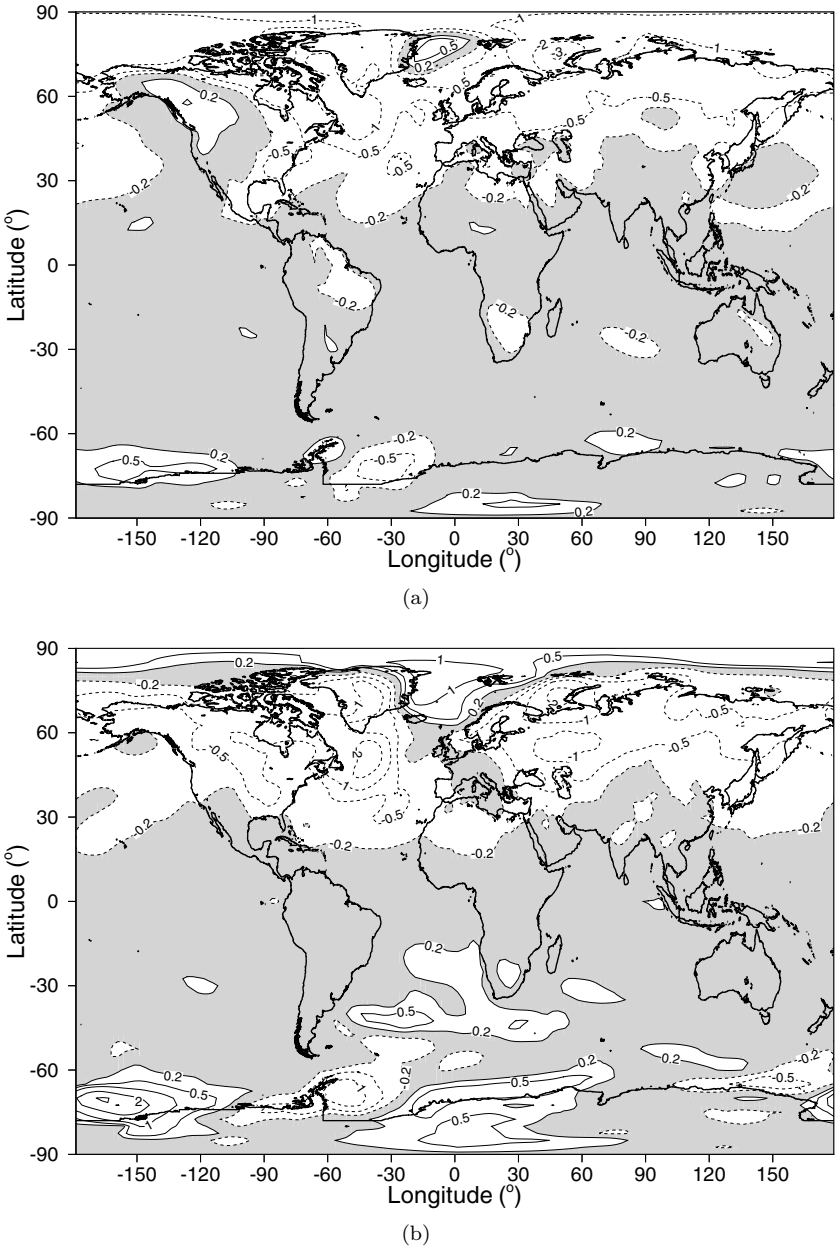

Fig 9. Difference (FW–CTRL) in the annual mean averaged air temperature for years 11–50 (a) and years 111–150 (b). Contour isolines are 0.2, 0.5, 1 and 2°C.

Greenland–Scotland ridge, there is a rapid decrease in the total southward outflow from the Nordic Seas in FW over the first 20–30 yr of integration (Fig. 12b). This reduction is mainly caused by a reduced overflow between the Faroes and Scotland. There is also a fairly quick reduction in the net inflow across the ridge over the first 40 yr (Fig. 12a). However, for the rest of the period there is a gradual increase and subsequent stabilization of the flow across the ridge at a level just below CTRL. The most important reason for the intensified northward flow across the Greenland–Scotland ridge is the gradual increase (up to ∼0.5 Sv) in the net northward flow through the Faroe–Shetland Channel (Fig. 12a). This change is balanced by a reduced northward flow through the Bering Strait of about 0.3 Sv (Fig. 12a), and an increased southward flow through the Canadian Archipelago of about 0.2 Sv (Fig. 12b).

For the Barents Opening, the northward flow in FW decreases by more than 1 Sv over the first 30 yr. Thereafter, the flow gradually increases and reaches a value about 0.6 Sv below that of CTRL at the end of the integration. The net northward flow through the Fram Strait is fairly stable, with an indication of a slight increase (a few tenths of a Sv) during the second half of the integration. The change in the southward flow across the Fram Strait is larger, with a decrease of more than 1 Sv over the first 40 yr. For the period between years 50 and 100, the southward

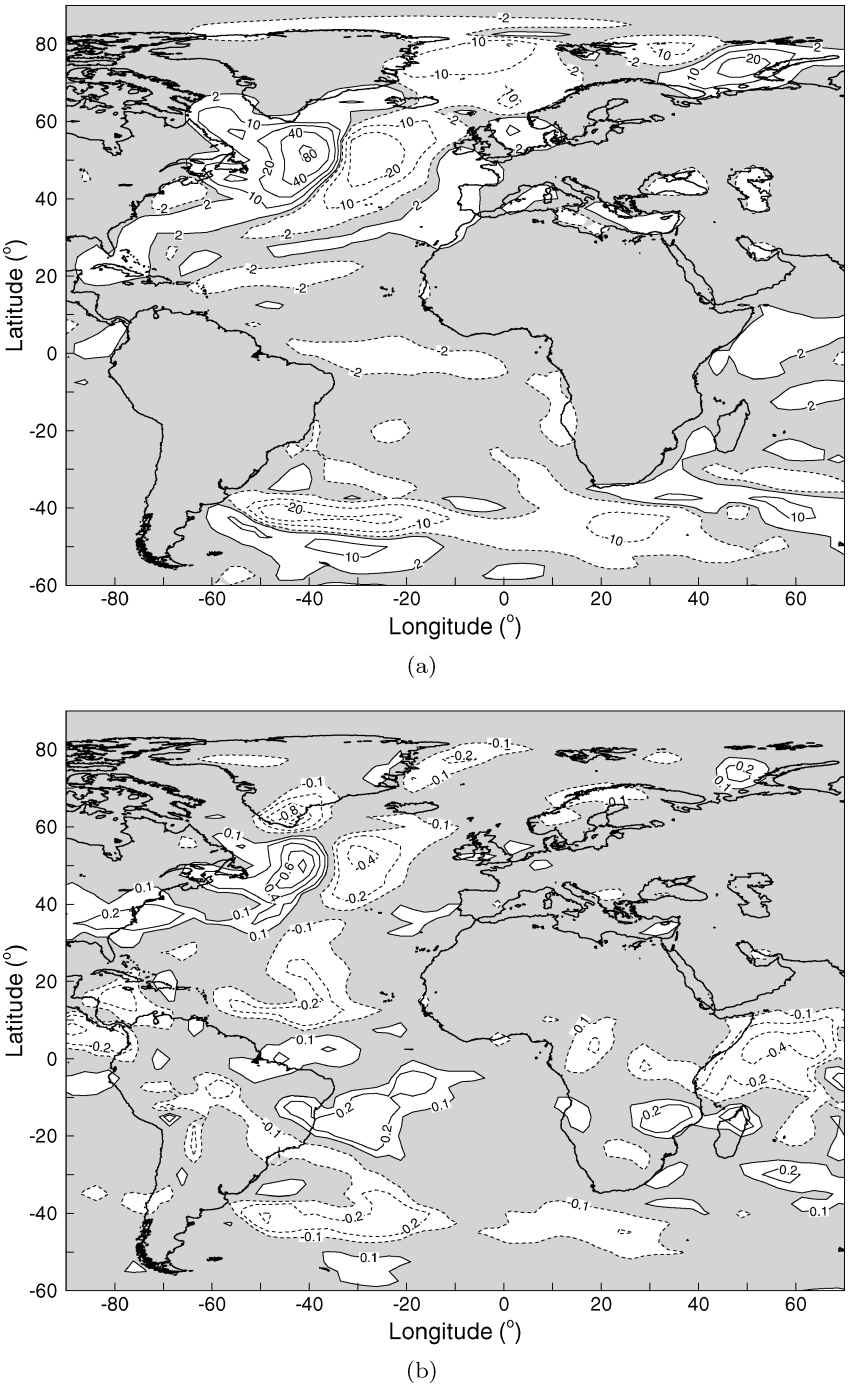

Fig 10. (a) Difference (FW–CTRL) in the mean surface heat flux (W m^{-2}) for the last 40 yr of the integration. Contour isolines are 2, 10, 20, 40 and 80 W m^{-2}. (b) As for (a), but for the P–E (mm d^{-1}) fluxes. Contour isolines are 0.1, 0.2 and 0.5 mm d^{-1}. Positive values mean a downward directed flux of heat (a) and freshwater (b).

flow through the Fram Strait in FW is about 1.3 Sv below that of CTRL, whereas the difference decreases to less than 1 Sv towards the end of the integration.

The unchanged or slightly increased northward flow of water through the Fram Strait (Fig. 12a), in combination with the increased temperature of the Atlantic Water in the region towards the end of the integration (Fig. 5b), leads to a gradual increase in the northward transport of heat through the passage (Fig. 13a). For the Barents Opening, a reduced northward transport of heat of about 20 TW (1 TW = 10^{12} W) is found for the first 60 yr, with a subsequent recovery over the rest of the period. Across the Greenland–Scotland ridge, the heat transport is reduced by about 40 TW over the first 50 yr. Most of this reduction occurs across the Denmark Strait and between Iceland and the Faroes, while the heat transport between the Faroes and Scotland is only slightly reduced (not shown). The rest of the period is

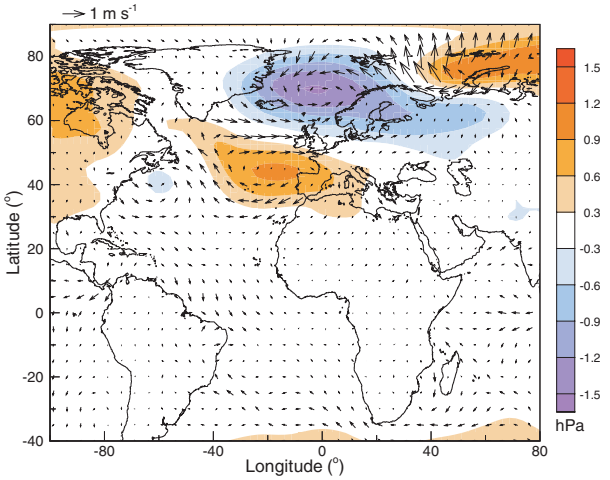

(a)

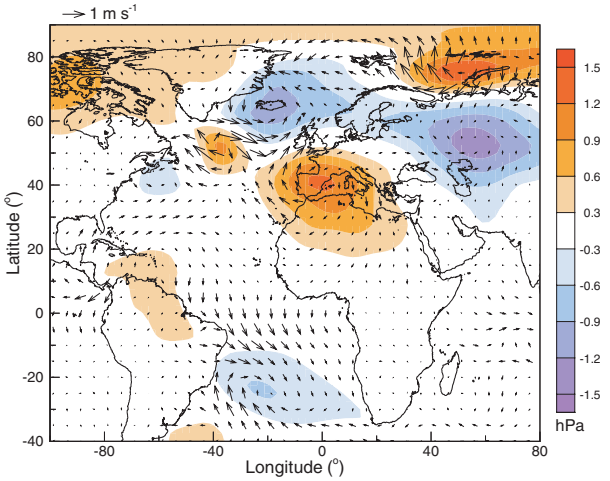

(b)

Fig 11. Changes (FW − $\overline{\text{CTRL}}$, where $\overline{\text{CTRL}}$ is the average over CTRL) of the winter (DJF) sea level pressure (hPa) and wind field (m s^{-1}) averaged over the years 11–50 (a) and 51–150 (b). The contour interval is 0.3 hPa. The reference vector is shown in the upper-left part of the panels.

characterized by a recovery and subsequent increase in the heat transport to the Nordic Seas. This increase is mainly caused by the increased inflow of Atlantic Water between the Faroes and Scotland (Fig. 12a).

An illustration of how the anomalous freshwater is transported out of the Arctic Mediterranean is provided by freshwater transports across the key sections in the region. The freshwater transport (F_t; m^3 s^{-1}) is defined as

$$F_t = \frac{S_{ref} - \overline{S}}{S_{ref}} \overline{F}_v, \tag{1}$$

where $\overline{S}$ (psu) and $\overline{F}_v$ ($m^3 s^{-1}$) are the upper 200 m averaged salinity and volume transports, respectively, and $S_{ref} = 33.4$ psu is a reference salinity computed as the mean salinity of the upper 200 m of the Nordic Seas and the Arctic Ocean in FW. Changes in the freshwater transports out of the Arctic Mediterranean are shown in Fig. 13b. The reduced northward volume transport across the Bering Strait plays a minor role in the net freshwater transport budget. On the other hand, the freshwater transport across the Canadian Archipelago increases steadily to a level about 0.02 Sv above CTRL. Early in the period, the freshwater transport across the Greenland–Scotland ridge is dominant, with increases of 0.04 and 0.12 Sv for the Denmark Strait and the Iceland–Scotland ridge, respectively. However, towards the end of the period the freshwater transport across the Greenland–Scotland ridge diminishes and the relative importance of the Canadian Archipelago increases.

3.5. *Ocean general circulation response*

The main changes in the general ocean circulation in the North Atlantic–Arctic Ocean can be deduced by examining the difference in the sea surface height between CTRL and FW (Fig. 14). Three changes are of particular importance. First, the North Atlantic Drift follows a more easterly path across the central North Atlantic in FW. Secondly, the circulation in the Barents Sea is fundamentally changed. In CTRL, the Atlantic Water flowing through the Barents Opening enters the Arctic Ocean mainly through the St Anna Trough. In FW, the main escape route is between Spitsbergen and Franz Josef Land. Thirdly, the clockwise circulation pattern within the Arctic Ocean is generally intensified.

Large-scale anomalies in the wind stress field will alter the frictional balance and cause an immediate response in the upper wind-driven circulation. The upper layer vertical integral of the horizontal flow, the Ekman transport (M_{ek}; m^2 s^{-1}), is governed by the wind stress anomaly $\boldsymbol{\tau}_a$ (kg m^{-1} s^{-2}), a reference density ρ_0 (kg m^{-3}) and the Coriolis parameter f (s^{-1}):

$$M_{ek} = (-\boldsymbol{k} \times \boldsymbol{\tau}_a)/(\rho_0 f),$$

where $\boldsymbol{k}$ is a unit vector in the vertical.

The Ekman part Φ (m^3 s^{-1}) of the AMOC response to changes in the wind forcing can be found by zonally integrating M_{ek} (Visbeck et al., 2003):

$$\Phi = \int M_{ek} \mathrm{d}x.$$

The Ekman transport for CTRL averaged over the entire 150-yr period show a transport towards the equator north of about 30°N, and a poleward transport south of 30°N (not shown). Figure 15a shows the Ekman induced zonally averaged overturning (Φ) expected for positive and negative NAO phases in CTRL. For a positive NAO phase, the poleward surface transport is reduced by about 2.5 Sv at 55–60° and enhanced by about 1 Sv at about 35°N. For a negative NAO phase, the situation is almost reversed.

The changes in the Ekman transport in FW are examined over two different periods: years 11–50 (P1) and years 51–150 (P2).

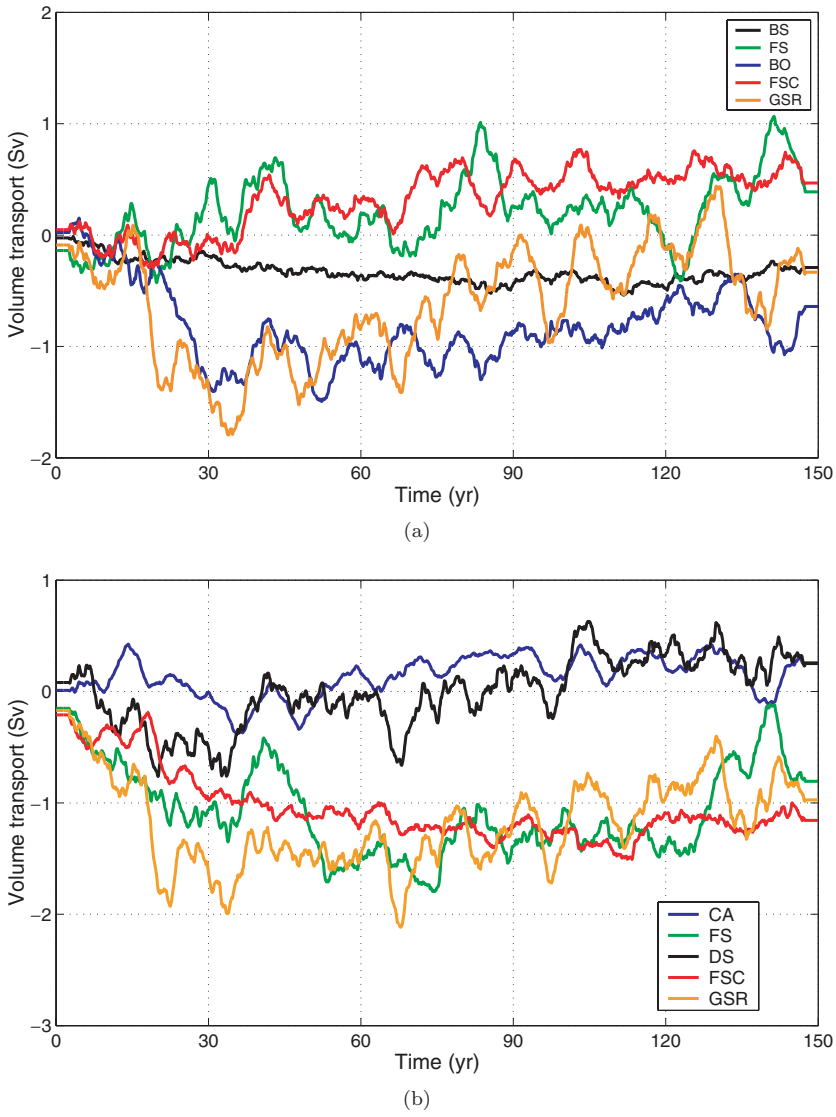

Fig 12. Changes in the volume transports (Sv) in and out of the Arctic Mediterranean. (a) Time series of the northward volume transport anomaly (FW–CTRL) through the Bering Strait (BS; black line), Fram Strait (FS; green line), Barents Opening (BO; blue line), Faroe–Shetland Channel (FSC; red line) and the Greenland–Scotland ridge (GSR; orange line). (b) Time series of the southward transport anomaly through the Canadian Archipelago (CA; blue line), FS (green line), Denmark Strait (DS; black line), FSC (red line) and the GSR (orange line). All time series are smoothed using a 5-yr running mean filter.

For P1, the Ekman induced zonally averaged overturning is increased between 25 and 45°N, and reduced poleward of 45°N (Fig. 15b). This pattern bears a strong resemblance to the pattern found for positive NAO phases in CTRL (Fig. 15a). The largest deviations are found at 30°N (+0.1 Sv) and at about 55°N (−0.6 Sv). In P2, there is a general increase in the Ekman contribution to the AMOC poleward of 40°N compared to P1, with maximum contribution of about 0.4 Sv at 50°N (Fig. 15b). A comparison of P1 and P2 across the Greenland–Scotland ridge (dotted line in Fig. 15a) shows an increased Ekman contribution to the AMOC of about 0.2 Sv in P2 compared to P1.

4. Discussion

The high latitude coupled atmosphere–sea-ice–ocean system is highly non-linear as localized changes in one component have the potential to generate significant changes on regional to hemispheric or even global scales in other components. For instance, numerical experiments indicate that SST and sea-ice extent anomalies in a region confined to the Labrador Sea have the potential to affect the average and synoptic atmospheric circulation at mid to high northern latitudes (Deser et al., 2000; Kvamstø et al., 2004). Furthermore, the absence of formation of deep-water masses in the Atlantic subpolar gyre or in the Nordic Seas may lead to a reduced strength of the Atlantic, and possibly the global, thermohaline circulation. Several hypotheses have been put forward to describe mechanisms for the apparent instantaneous (of the order of a few yr) onset of the AMOC (Dokken and Jansen, 1999; Ganopolski and Rahmstorf, 2001) and the global-scale climatic consequences thereof.

In the following, we present an interpretation of the obtained responses of the applied freshwater anomaly to the Nordic Seas

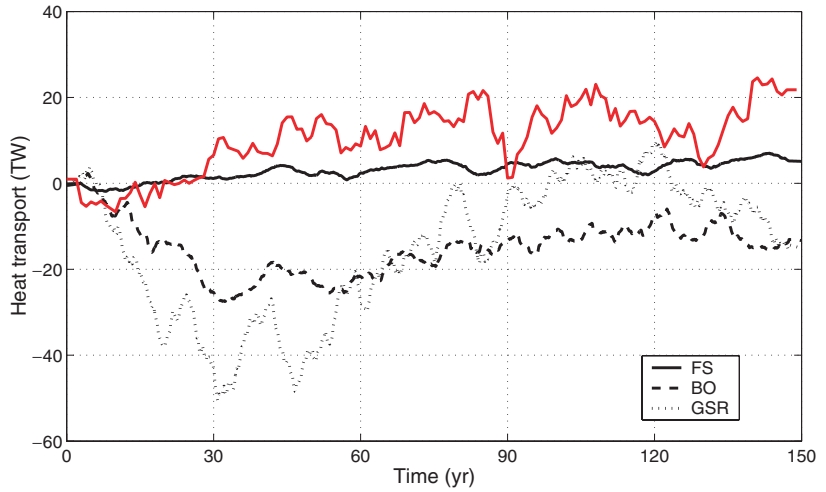

(a)

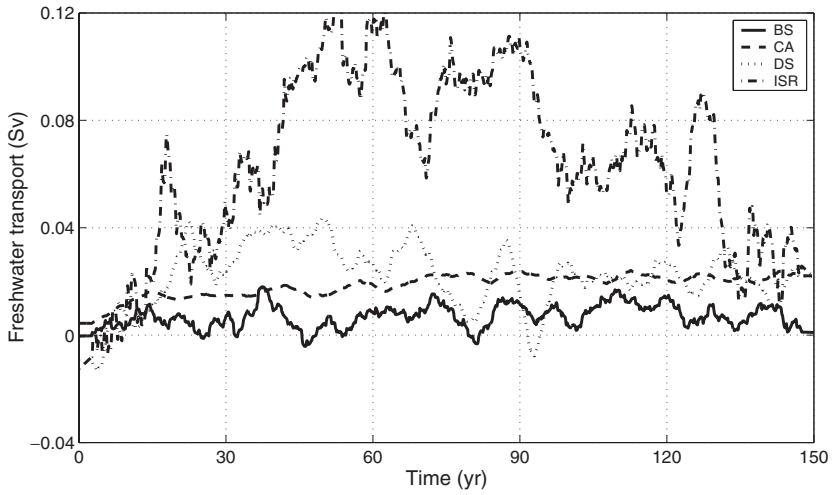

(b)

Fig 13. Changes in the heat (TW) and freshwater (Sv) transports for the Arctic Mediterranean. (a) Time series of the northward heat transport anomaly (FW–CTRL) through the Fram Strait (FS; solid line), Barents Opening (BO; dashed line) and the Greenland–Scotland ridge (GSR; dotted line). In addition, the difference (FW–CTRL) in the heat lost to the atmosphere during convection in winter (December–May) in the West Spitsbergen Current is shown in red. (b) Time series of the southward freshwater transport anomaly (Sv) through the Bering Strait (BS; solid line), Canadian Archipelago (CA; dashed line), Denmark Strait (DS; dotted line) and the Iceland–Scotland ridge (ISR; dash-dotted line). All time series are filtered using a 5-yr running mean.

and the Arctic Ocean. The discussion is split into a discussion of the thermohaline and wind-driven responses. Such a split is somewhat artificial as the system is coupled on a variety of spatial and temporal scales, implying intricate cause–effect and damping–growing interactions and feedbacks.

4.1. Thermohaline forced response

It is a common finding from simplified and coupled atmosphere–sea-ice–ocean models that the strength of the AMOC reduces if there is a net flux of freshwater added to high northern latitudes (Manabe and Stouffer, 1997; Schiller et al., 1997; Vellinga et al., 2002). This result is consistent with the scaling (Welander, 1986; Nilsson and Walin, 2001)

$$M_G \propto \Delta\rho_G H^2,$$

where M_G is the poleward volume transport, $\Delta\rho_G$ is the equator-to-pole density difference, and H is the thickness of the upper branch of, in our case, the AMOC.

The above scaling is consistent with FW for the first 50 yr of the integration: the maximum AMOC drops from about 18 to 12 Sv as a response to the freshwater supplied to the high northern latitudes. A result of the added freshwater is that the formation of intermediate and deep-water masses within the Nordic Seas is reduced (Fig. 2b). In addition, there is a reduction in the southward subsurface flow through the Fram Strait of about 1.5 Sv (Otterå et al., 2003). The reduced southward flow across the Greenland–Scotland ridge of 1.5–1.7 Sv during the first 30 yr of FW (Fig. 12b) is therefore caused by a combination of reduced deep-water formation within the Nordic Seas and reduced southward flow through the Fram Strait. A strong reduction in the deep-water formation in the Labrador and Irminger Seas (Fig. 2b), in combination with the reduced overflow from the Nordic Seas, implies a reduced intensity of the AMOC in FW. This is particularly the case over the first 50 yr of the integration. Somewhat counteractive, however, the AMOC in FW starts to recover after 50 yr, and nearly reaches

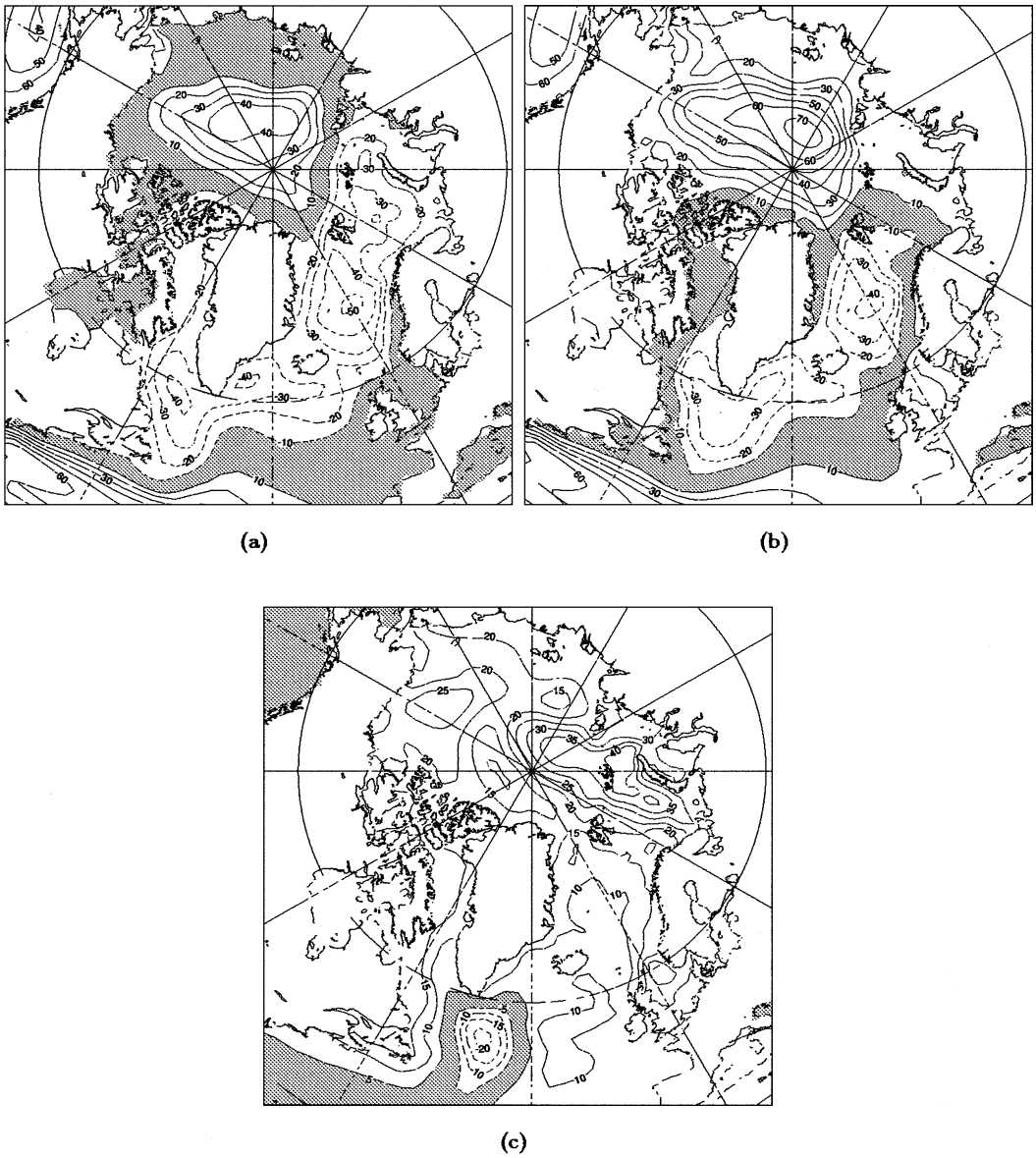

Fig 14. The sea surface height (cm) averaged over the last 40 yr of integration for CTRL (a), FW (b) and FW–CTRL (c). The contour interval is 10 m (a), (b) and 5 m (c).

the maximum strength of the AMOC in CTRL at the end of the experiment.

One of the processes driving the recovery of the AMOC can be examined by evaluating the evolution of surface density. The equator-to-pole density difference drops rapidly over the first 30–40 yr, mainly due to the freshening in the subpolar region (Fig. 16a). Over the last 100 yr there is a fairly stable equator-to-pole density difference, caused by about similar density variations in the subpolar and WTNA regions.

In the WTNA region, the surface density is generally increased over the first 90 yr (Fig. 16a). Otterå et al. (2003) showed that these anomalies are the result of reduced surface and subsurface velocities of up to 25% along the northern coast of the South American continent. The convergence of the northward surface flow and subsequent increased residence time of the surface and subsurface waters implies increased heat and salt content of the water masses in the WTNA. Gradually, these anomalously saline low latitude waters expand north-eastward by dispersive mixing and advective transport (Fig. 5a).

By separating the density anomalies for the subpolar and WTNA regions into the thermal and haline expansion terms, the relative importance of temperature and salinity on the density variations can be examined (Figs. 16b and c). In the North Atlantic subpolar region, density variations are almost entirely determined by variations in salinity (Fig. 16b). The salt advected into this region therefore influences the density directly. In both

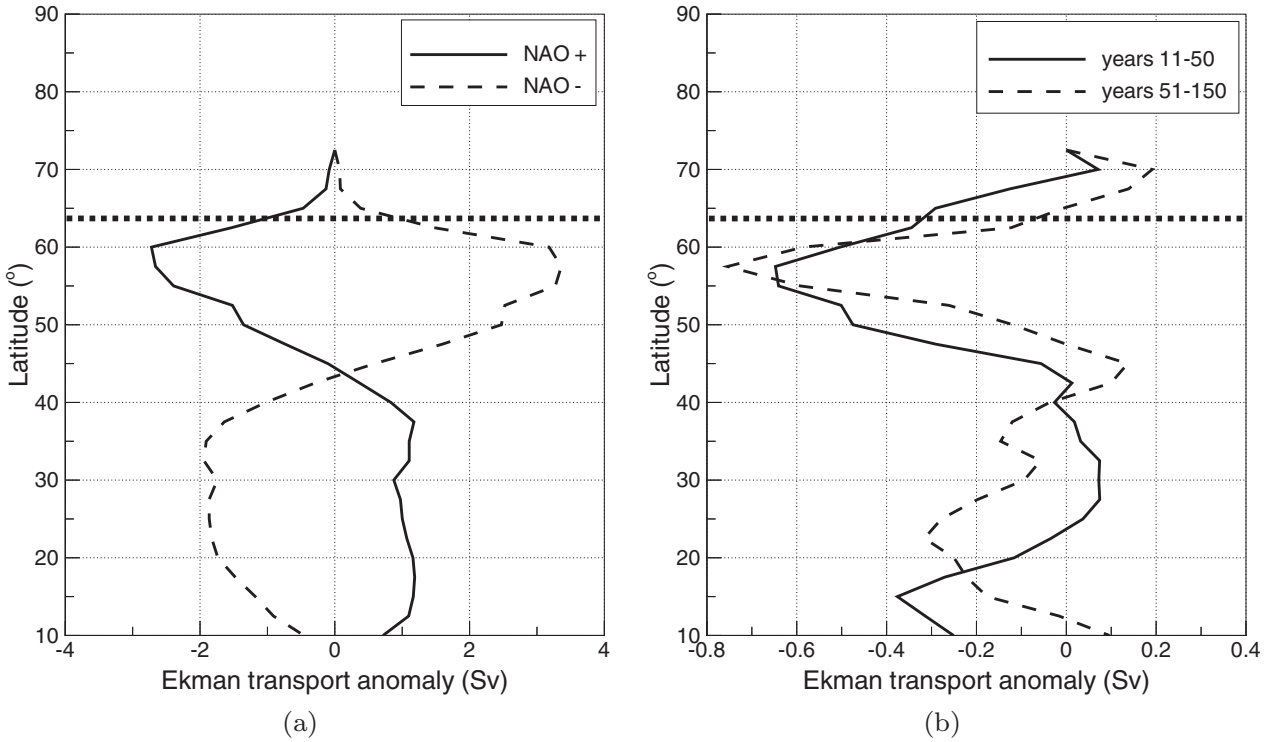

Fig 15. (a) Zonally integrated Ekman transport anomaly (meridional component; Sv) for positive (solid line) and negative (dashed line) NAO index phases in CTRL. The anomaly is calculated as the difference between the mean Ekman transport for the entire period and the composite of years of the NAO index exceeding ±1 std. (b) Zonally integrated Ekman transport anomaly (FW − $\overline{\text{CTRL}}$, where $\overline{\text{CTRL}}$ is the mean of the whole period) for winter (DJF) in years 11–50 (P1, solid line) and years 111-150 (P2, dashed line). Negative values indicate that the Ekman transport acts to reduce the AMOC.

the Labrador and the Irminger Seas, an increase in the winter mixing is found between years 50–80 as a result of increased surface water density (Fig. 2b), leading to an intensification of the AMOC. Over the last 50 yr of the integration, the transport of salt can no longer counteract the continuous supply of freshwater to the Labrador Sea, leading to reduced winter mixing (Fig. 2b) and increased sea-ice extent (Fig. 8) here. The Irminger Sea region receives, however, sufficient saline waters from the WTNA region to counteract the artificially released freshwater (Fig. 5a). This, in combination with enhanced westerlies over the region (Fig. 11), leads to a gradual increase in the formation rate of dense water masses in the Irminger Sea region (Fig. 2b).

Conceptually, the AMOC may be considered as an overturning circulation with narrow sinking at high latitudes and broad upwelling at low latitudes. Presently, the general view is that the rate limiting branch of the AMOC is the upwelling of dense water, rather than the deep-water formation at high latitudes (e.g. Marotzke and Scott, 1999; Huang, 1999). The strength of vertical mixing in the World Ocean is, however, poorly known. Scaling arguments using simple one-hemispheric ocean models suggest that the strength of the AMOC (say ψ) obeys (e.g. Welander, 1986)

$$\psi \sim \Delta\rho_G^{1/3}\kappa^{2/3},$$

where κ (m^2 s^{-1}) is the vertical diffusivity. If κ is fixed, the strength of the AMOC would obviously increase with an increased density difference.

In the ocean, however, the vertical diffusivity presumably depends on the vertical density stratification, which in turn is coupled to $\Delta\ \rho_G$. Accordingly, a change in $\Delta\rho_G$ will also imply a change in κ. Using an analytical two-layer model of the AMOC, Nilsson and Walin (2001) found that if the vertical diffusivity increases with decreasing stratification, then the AMOC may in fact increase in response to a reduced equator-to-pole density difference. This result contradicts the established view, which is based on the assumption that the vertical diffusivity is independent of the vertical density stratification.

In the BCM, the diapycnal mixing coefficient is given by $3 \times 10^{-7}\ N^{-1}$ (m^2 s^{-1}), where N (s^{-1}) is the Brunt–Väisälä frequency. Hence, the diapycnal mixing increases with decreasing vertical density stratification. Because of reduced formation of dense water masses in the northern North Atlantic, as is the case for FW, the vertical density stratification in the Atlantic Ocean weakens with time. The zonally averaged changes in the strength of the diapycnal mixing are shown in Fig. 17 for three different time periods. Early in the integration (years 31–50) no significant changes in the diapycnal mixing are found (Fig. 17a).

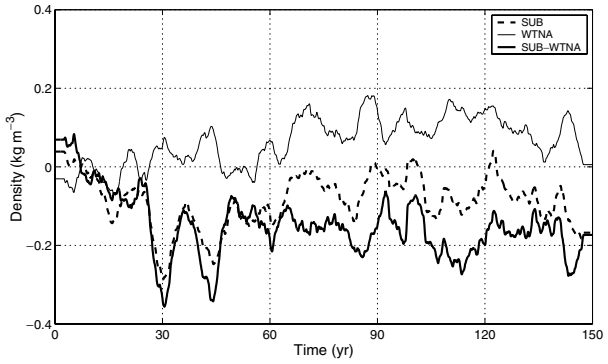

(a)

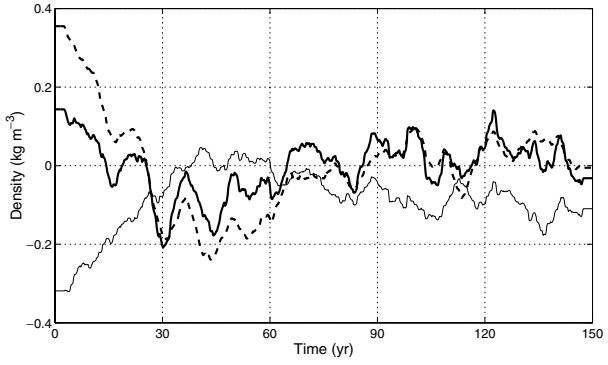

(b)

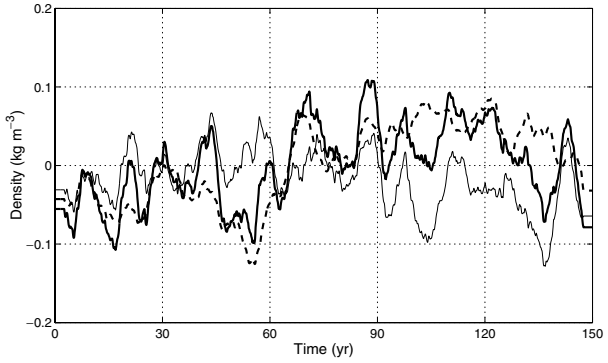

(c)

Fig 16. (a) Time series of the surface density anomalies (kg m^{-3}) in the subpolar (SUB) region (45°N–60°N and 60°W–30°W; dashed line), the WTNA region (0°N–30°N and west of 40°W; thin solid line), and the difference (SUB–WTNA; thick solid line). The density anomalies in FW (FW $-$ $\overline{\text{FW}}$, where $\overline{\text{FW}}$ is the mean over FW) are shown in (b) and (c) for the SUB and WTNA regions, respectively. Together with the actual density anomalies (thick solid lines) are the contributions from the temperature (thin solid line) and salinity (dashed line) anomalies.

For years 71–90, the diapycnal mixing in FW increases by 5–10% over large parts of the Atlantic Ocean, with even stronger increases (in excess of 20%) in the subpolar Atlantic (Fig. 17b). Towards the end of the integration (years 131–150) the diapycnal mixing has diminished, but there is still an increased mixing of 5–10% at intermediate depths in most of the Atlantic, and high values (15–20%) in the subpolar Atlantic (Fig. 17c).

Scaling arguments and numerical simulations give that the diapycnal upwelling is proportional to N^{-1} for a diapycnal mixing coefficient proportional to N^{-1} (Nilsson and Walin, 2001; Nilsson et al., 2003). Consistent with sensitivity experiments with MICOM (Gao et al., 2003), the basin-scale increase in diapycnal mixing of about 5–10% is estimated to directly contribute about 1 Sv to the overall recovery of the AMOC in FW.

4.2. Wind forced response

Despite the fact that the maximum AMOC is weakened by about 6 Sv over the first 50 yr of FW, the northward flow of Atlantic Water between the Faroes and Scotland remains unchanged and even increases throughout the integration (Fig. 12a). This response is the direct reason for the small changes in SSS and the increased SSTs in the central Nordic Seas in FW (Fig. 5).

The freshwater transported through the Canadian Archipelago acts as an effective barrier for deep winter mixing in the Labrador Sea, resulting in a quick expansion of the sea-ice in the region. It is well documented that there is a tight coupling between the wind fields in the Atlantic–European region and the Labrador sea-ice (Deser et al., 2000). Furthermore, Kvamstø et al. (2004) show that anomalies in sea-ice and SST in the Labrador Sea region influence the SLP in the North Atlantic–Europe region. In the latter study, performed with idealized SST and sea-ice forcing fields as boundary conditions for the atmosphere-only component of the BCM, colder than normal conditions in the Labrador Sea region lead to a weakened Icelandic Low, and by that to a circulation regime with a low NAO index.

The resulting change in the atmospheric circulation in FW is associated with a general increase in the SLP difference between the Nordic Seas and the Azores, implying an overall more positive NAO-like state (Fig. 11), despite the colder than normal conditions in the Labrador Sea region in FW. The NAO response in the BCM is thus opposite to the response obtained from the atmosphere-only experiments reported by Kvamstø et al. (2004). The same conclusion was obtained when the SST and sea-ice fields extracted from the last 40 yr of FW were used as boundary conditions for the atmosphere component of the BCM (not shown). These findings strongly support the presence of a coupled NAO-like atmosphere–sea-ice–ocean response mode triggered by the freshwater input in FW.

The intensified westerlies in the northern North Atlantic and strengthened northerlies along the western part of the Nordic Seas force the North Atlantic Drift to follow a more easterly path in FW, which in turn forces a strong asymmetric response in the northern North Atlantic SST (Fig. 5b) and heat and freshwater fluxes (Fig. 10). Nilsen et al. (2003) found a strong correlation between the flow of Atlantic Water into the eastern part of the central Nordic Seas and a SLP pattern with a low-pressure system over the Nordic Seas and a high-pressure system with centre

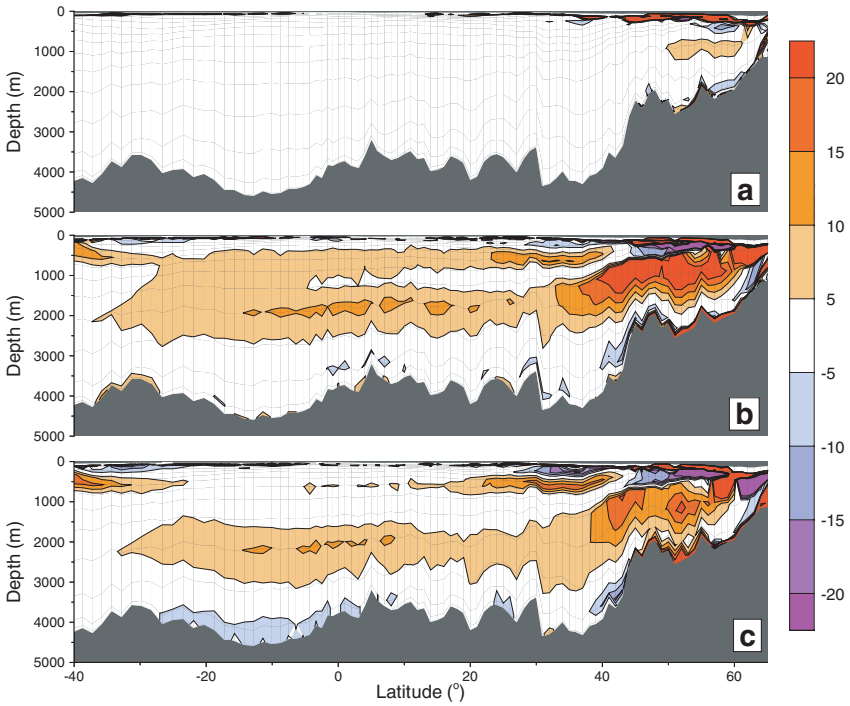

Fig 17. Changes (in per cent) in FW compared to CTRL of the zonally averaged values of the diapycnal mixing in the Atlantic Ocean for years 31–50 (a), years 71–90 (b) and years 131–150 (c). Positive values indicate increased diapycnal mixing.

of action in the vicinity of the Azores. Similar correlations are found in CTRL (not shown). The increased transport between the Faroes and Scotland in FW (Fig. 12a) can therefore partly be explained by the SLP anomalies found in FW. The net result of this change is that more warm Atlantic Water is transported into the eastern part of the Nordic Seas leading to a general warming of the Nordic Seas (Figs. 5b and 13a).

An additional mechanism for maintaining the flow of Atlantic Water into the Nordic Seas is linked to a higher sea surface height in the Arctic (Otterå and Drange, 2004). This is a geostrophic effect of the freshening in the Arctic and it leads to reduced inflow through the Bering Strait and enhanced outflow through the Canadian Archipelago. These volume flux changes are then compensated by increased inflow to the Nordic Seas. In the northern North Atlantic, there is also an increase in the Ekman contribution to the AMOC over the last 100 yr of 0.1–0.4 Sv (Fig. 15b), which also contributes to the recovery of the AMOC.

In the Barents Sea, the freshwater intrusion and the advancing sea-ice have an immediate impact on the atmosphere, with stronger south-easterly wind anomalies between Svalbard and Franz Josef Land. As a consequence, the Barents Sea branch of Atlantic Water is suppressed while the inflow of Atlantic Water with the West Spitsbergen Current through the Fram Strait is enhanced. Furthermore, the retreat of sea-ice in the region of the Fram Strait and along the coast of Greenland (Fig. 8b), together with increased SSTs in the Nordic Seas, result in heat fluxes from the ocean to the atmosphere of about 10–15 W m^{-2} in the region. This heat leads to a gradual warming of the Arctic region in FW (Fig. 9). The importance of the change in oceanic heat transport for this warming is estimated by the red curve in Fig. 13a. There is a linear increase in the supply of heat to the atmosphere in the region south-west of Spitsbergen until year 50, and a fairly steady supply of heat thereafter. The increased transfer of heat from the ocean to the atmosphere in FW reaches about 15 TW in year 50. This is 30% of the heat that enters the Barents Sea in CTRL, and 20–25% of the estimated net transport of heat into the Barents Sea (Simonsen and Haugan, 1996).

Another striking feature in FW is the southward shift of the ITCZ in the equatorial Atlantic. This shift is reflected in the precipitation–evaporation (P–E) and wind responses (Figs. 10b and 11b, respectively), and leads to longer residence time and reduced precipitation to the water masses here. This will in turn contribute to the formation of salt anomalies in this region.

4.3. *Comparison to paleo records*

The evolution of the temperature of the upper 1000 m of the water column in the Guyana Current (Fig. 7) shows a subsurface warming of about 0.2°C (0.4°C) around year 30 (70). The warming persists throughout most of the integration. This finding suggests that a reduced AMOC is associated with a warming of the upper 1000 m of the WTNA in agreement with the findings of Manabe and Stouffer (1997). While the high northern latitudes experience a general cooling (e.g. Fig. 9), the WTNA waters warm.

The out-of-phase operation of the tropical and high-latitude Atlantic temperatures is consistent with paleo records of the oceanic responses during the rapid climate changes of the last

deglaciation. Using a high temporal resolution record of SSTs from the WTNA, Rühlemann et al. (1999) found significant warming during the Heinrich event H1 (16 900–15 400 calendar years BP) and the Younger Dryas event (12 900–11 600 calendar years BP), both periods in which intense cooling took place at high northern latitudes. Although FW clearly does not represent deglacial conditions, the experiment does highlight the potential importance of the WTNA for detecting large-scale changes in the past.

4.4. *Comparison with similar studies*

A common finding from freshwater experiments with other climate models (e.g., Manabe and Stouffer, 1997; Schiller et al., 1997; Rind et al., 2001; Vellinga et al., 2002) is that the AMOC is shut down or severely reduced in response to strong high-latitude freshwater forcing. The freshwater simulation reported here, however, show a different behaviour: after an initial decline, the AMOC nearly recovers its original strength despite the steady supply of anomalous freshwater to the high-latitude seas. A natural question is therefore what causes the BCM to behave differently.

One explanation could be differences in the model formulations. As opposed to other climate models, which commonly use geopotential ocean models, the ocean component of the BCM, MICOM, is formulated in an isopycnic framework. Furthermore, the vertical diffusivity in MICOM is vertical stratification dependent. This parametrization differs from most other climate models, which usually assume a time-invariant vertical diffusivity. Because of the increased high-latitude freshwater input, there is a weakening of the vertical density stratification in the North Atlantic. In the BCM this leads to increased diapycnal mixing (Fig. 17) and upwelling over large parts of the Atlantic basin, and subsequent to an intensification of the AMOC.

Another possible reason for the different response is related to different locations of the freshwater input. In model studies similar to that presented here, the anomalous freshwater is usually released to the north-western Atlantic, in contrast to the Nordic Seas and the Arctic Ocean as is the case here. Furthermore, in the present version of the BCM both the Bering Strait and the Canadian Archipelago are open for water transport, which is not always the case in other studies (e.g. Manabe and Stouffer, 1997; Schiller et al., 1997). For instance, the increased sea surface height in the Canadian Basin in FW (Fig. 14) leads to reduced inflow across the Bering Strait and increased southward transport of water across the Canadian Archipelago (Fig. 12). To compensate for this loss of water, the poleward transport of water across the Greenland–Scotland ridge would have to increase. This mechanism has also been observed in a freshwater experiment conducted with a regional version of MICOM (Otterå and Drange, 2003). The increased inflow of Atlantic Water across the Faroe–Shetland Channel towards the end of the integration therefore probably has a compensating component as well as a wind-induced component.

An important mechanism for the recovery of the AMOC is the generation of the WTNA salt anomalies (Fig. 6). In Otterå et al. (2003), these anomalies were explained by increased residence time of the surface waters transported with the AMOC of the South American continent. However, a relocation of the equatorial precipitation belt further south could also be important. Both Schiller et al. (1997) and Vellinga et al. (2002) found a southeastward shift of the ITCZ in similar freshwater experiments. In Vellinga et al. (2002), this created positive salt anomalies in the tropical North Atlantic, which was advected northward by the subtropical gyre and led to a recovery of the AMOC. The dipole pattern in the atmospheric freshwater flux anomalies in the equatorial Atlantic (Fig. 10b) and the northerly wind anomalies across the equator (Fig. 11b) indicate that a similar mechanism is operating in the BCM.

In the simulation by Latif et al. (2000), anomalously high salinities in the tropical Atlantic were obtained as a result of a strong and persistent El Niño-like forcing in the Pacific. However, no significant changes are detected in the El Niño characteristics in FW (not shown), excluding this mechanism as a possible cause for the WTNA salt anomaly in FW.

An important caveat of the presented experiment is the exclusion of thermobaric effects in MICOM. As a consequence, the model cannot represent the generation of Antarctic bottom water in the Southern Ocean. This model deficiency could make the AMOC too insensitive to high-latitude buoyancy forcing. In future versions of the BCM, thermobaric effects will be included. It should also be noted that the applied flux adjustment fields tend to keep the model climatology closed to the observed climatology. Whether or not the use of flux adjustment fields may change the model sensitivity to freshwater perturbations is an open question, although Schiller et al. (1997) concluded that this is not likely the case.

Finally, it should be noted that several key characteristics of the Atlantic–Arctic climate system in CTRL are represented realistically. This is, in particular, the case for the volume fluxes of water into and out of the Arctic Mediterranean (Otterå et al., 2003), the extent of sea-ice in the Arctic (Fig. 8), and the NAO variability (Furevik et al., 2003).

4.5. *Quantification of the recovery*

The recovery of the AMOC of about 4 Sv is governed by different processes, all of which are hard to quantify in terms of changes in the meridional volume fluxes. However, the presented analyses give indications of the relative importance of the different processes. Based on this, it is argued that the enhanced diapycnal mixing contributes about 1 Sv, while the enhanced winter mixing in the subpolar North Atlantic contributes about 1.5 Sv (Fig. 2b, red curve). Furthermore, the outflow from the Nordic Seas contributes with about 0.8 Sv (plus entrainment of ambient

waters downslope of the Greenland–Scotland ridge that is hard to assess), and the wind-induced Ekman transport contribute with a few tenths of Sv. In addition, the enhanced volume flux through the Canadian Archipelago of about 0.3 Sv will also influence the strength of the AMOC.

5. Concluding remarks

In the present study, a number of complex feedback mechanisms within the atmosphere–ocean–sea-ice system have been identified. For the present-day climate state, the strength of the AMOC is found to be quite robust to the isolated effect of enhanced high-latitude freshwater forcing, at least on a centennial time-scale. Another important finding is the coupling between tropical heat and salt anomalies and high-latitude mixing. In particular, the recovery and subsequent increase in winter mixing in the Irminger Sea is crucial for the recovery of the AMOC.

Furthermore, changes in the wind-driven circulation are found to support the recovery of the AMOC over the last 100 yr, particularly in the northern North Atlantic. The anomalous freshwater input also appears to trigger a coupled NAO-like atmosphere–sea-ice–ocean response mode, which in turn maintains an asymmetric SST pattern in the northern North Atlantic. In addition, a possible response of the AMOC to the density stratification dependent diapycnal mixing currently used in the BCM has been identified. Such a choice of parametrization for the diapycnal mixing is more elaborate than fixed values used in most of the present-day climate OGCM (Nilsson and Walin, 2001). However, additionally experiments need to be conducted to quantify in more detail the effect of density stratification dependent mixing on the AMOC.

Finally, the gradual warming of the thermocline in the Guyana Current during the period with reduced AMOC and cooling at the high latitudes supports observations from the last deglaciation inferred from paleo records (Rühlemann et al., 1999). The warming of low-latitude Atlantic intermediate-depth waters could therefore possibly serve as an indicator of a possible reduction in the AMOC also in the future. A combination of paleo records from the past climate, instrumental observations of the present climate and experiments with models of different type and complexity are certainly needed to reduce the uncomfortably large uncertainty in the present knowledge of the future evolution of the AMOC (Houghton et al., 2001).

6. Acknowledgments

This study has been supported by the Research Council of Norway through a personal grant to OHO, through RegClim and NOClim (HD), KlimaProg's 'Spissforskningsmidler' (MB) and the Programme of Supercomputing, by the National Natural Science Foundation of China under grant 40125014 (DJ), by the EU-project PREDICATE (EVK2-CT-1999-00020), and by the G. C. Rieber Foundations. The authors are grateful to the BCM group for help and guidance. Comments and suggestions from two anonymous reviewers are highly appreciated. This is publication No. A43 of the Bjerknes Centre for Climate Research.

References

Aagaard, K. and Carmack, E. C. 1989. The role of sea-ice and other fresh water in the Arctic Circulation. *J. Geophys. Res.* **94**, 14 485–14 498.

Bentsen, M., Drange, H., Furevik, T. and Zhou, T. 2004. Simulated variability of the Atlantic Meridional Overturning Circulation. *Climate Dyn.* in press.

Bleck, R., Rooth, C., Hu, D. and Smith, L. T. 1992. Salinity-driven thermocline transients in a wind- and thermohaline-forced isopycnic coordinate model of the North Atlantic. *J. Phys. Oceanogr.* **22**, 1486–1505.

Bossuet, C., Déqué, M. and Cariolle, D. 1998. Impact of a simple parametrization of convective gravity-wave drag in a stratosphere-troposphere general circulation model and its sensitivity to vertical resolution. *Ann. Geophys.* **16**, 238–249.

Broecker, W. S. 1997. Thermohaline circulation, the Achilles heel of our climate system: will man-made CO_2 upset the current balance? *Science* **278**, 1582–1588.

Broecker, W. S., Peteet, D. and Rind, D. 1985. Does the ocean-atmosphere have more than one stable mode of operation? *Nature* **315**, 21–26.

Cubasch, U., Meehl, G. A., Boer, G. J., Stouffer, R. J., Dix, M. et al 2001. Projections of future climate change. In: *Climate Change 2001: The Scientific Basis: Contribution of Working Group I to the Third Assesment Report of the Intergovernmental Panel on Climate Change* (eds J. T. Houghton, Y. Ding, D. J. Griggs, M. Noguer, P. J. V. der Linden et al). Cambridge University Press, Cambridge.

Déqué, M., Dreveton, C., Braun, A. and Cariolle, D. 1994. The ARPEGE/IFS atmosphere model: A contribution to the French community climate modelling. *Climate Dyn.* **10**, 249–266.

Deser, C., Walsh, J. E. and Timlin, M. S. 2000. Arctic sea-ice variability in the context of recent wintertime atmospheric circulation trends. *J. Climate* **13**, 617–633.

Dokken, T. M. and Jansen, E. 1999. Rapid changes in the mechanism of ocean convection during the last glacial period. *Nature* **401**, 458–461.

Douville, H., Royer, J. F. and Mahfouf, J. F. 1995. A new snow parametrization for the Météo-France climate model. Part II: validation in a 3D GCM experiment. *Climate Dyn.* **12**, 37–52.

Drange, H. and Simonsen, K. 1996. *Formulation of air–sea fluxes in the ESOP2 version of MICOM*. Technical Report 125, Nansen Environmantal and Remote Sensing Center, Bergen, Norway.

Friedrich, H. and Levitus, S. 1972. An approximation to the equation of state for sea water, suitable for numerical ocean models. *J. Phys. Oceanogr.* **2**, 514–517.

Furevik, T., Bentsen, M., Drange, H., Kindem, I. K. T., Kvamstø, N. G. et al 2003. Description and validation of the Bergen Climate Model: ARPEGE coupled with MICOM. *Climate Dyn.* **21**, 27–51 (doi:10.1007/s00382-003-0317-5).

Ganopolski, A. and Rahmstorf, S. 2001. Rapid changes of glacial climate simulated in a coupled climate model. *Nature* **409**, 153–158.

Gao, Y., Drange, H. and Bentsen, M. 2003. Effects of diapycnal and isopycnal mixing on the ventilation of CFCs in the North Atlantic in an isopycnic coordinate OGCM. *Tellus* **55B**, 837–854.

Gaspar, P., Grégoris, Y. and Lefevre, J.-M. 1990. A simple eddy kinetic model for simulations of the oceanic vertical mixing: tests at Station Papa and Long-Term Upper Ocean Study Site. *J. Geophys. Res.* **95**, 16 179–16 193.

Harder, M. 1996. *Dynamik, Rauhigkeit und Alter des Meereises in der Arktis*. PhD Thesis. Alfred-Wegner-Institut für Polar- und Meeresforschung, Bremerhaven, Germany.

Hibler, W. D. 1979. A dynamic thermodynamic sea-ice model. *J. Phys. Oceanogr.* **9**, 815–846.

Houghton, J. T., Ding, Y., Griggs, D. J., Noguer, M., der Linden, P. J. V. et al eds. 2001. *Climate Change 2001: The Scientific Basis: Contribution of Working Group I to the Third Assesment Report of the Intergovernmental Panel on Climate Change*. Cambridge University Press, Cambridge.

Huang, R. X. 1999. Mixing and energetics of the oceanic thermohaline circulation. *J. Phys. Oceanogr.* **29**, 775–791.

Kvamstø, N. G., Skeie, P. and Stephenson, D. B. 2004. Impact extent of Labrador sea-ice oscillation on the North Atlantic atmospheric circulation. *Int. J. Climatology* **24**, 603–612.

Latif, M., Roeckner, E., Mikolajewicz, U. and Voss, R. 2000. Tropical stabilization of the thermohaline circulation in a greenhouse warming simulation. *J. Climate* **13**, 1809–1813.

Lott, F. 1999. Alleviation of stationary biases in a GCM through a mountain drag parametrization scheme and a simple representation of mountain lift forces. *Mon. Wea. Rev.* **125**, 788–801.

Manabe, S. and Stouffer, R. J. 1994. Multiple-century response of a coupled ocean–atmosphere model to an increase of atmospheric carbon dioxcide. *J. Climate* **7**, 5–23.

Manabe, S. and Stouffer, R. J. 1997. Coupled ocean–atmosphere model response to freshwater input: comparision to Younger Dryas event. *Paleoceanography* **12**, 321–336.

Marotzke, J. and Scott, J. R. 1999. Convective mixing and the thermohaline circulation. *J. Phys. Oceanogr.* **29**, 2962–2970.

Marotzke, J. and Stone, P. H. 1995. Atmospheric transport, the thermohaline circulation, and flux adjustments in a simple coupled model. *J. Phys. Oceanogr.* **25**, 1350–1364.

Nilsen, J. E. Ø., Gao, Y., Drange, H., Furevik, T. and Bentsen, M. 2003. Simulated North Atlantic–Nordic Seas water mass exchanges in an isopycnic coordinate OGCM. *Geophys. Res. Lett.* **30**, 1536 (doi:10.1029/2002GL016597).

Nilsson, J., Broström, G. and Walin, G. 2003. The thermohaline circulation and vertical mixing: does weaker density stratification give stronger overturning? *J. Phys. Oceanogr.* **33**, 2781–2795.

Nilsson, J. and Walin, G. 2001. Freshwater forcing as a booster of thermohaline circulation. *Tellus* **53**, 629–641.

Oki, T. and Sud, Y. C. 1998. Design of Total Runoff Integrating Pathways (TRIP) – a global river channel network. *Earth Interactions* **2**, 1–37.

Otterå, O. H. and Drange, H. 2004. *A possible feedback mechanism involving the Arctic freshwater, the Arctic sea-ice and the North Atlantic Drift. Adv. Atmos. Sci.*, accepted.

Otterå, O. H., Drange, H., Bentsen, M., Kvamstø, N. G. and Jiang, D. 2003. The sensitivity of the present-day Atlantic meridional overturning circulation to freshwater forcing. *Geophys. Res. Lett.* **30**, 1898 (doi:101029/2003GL017578).

Räisänen, J. 2001. CO_2-induced climate change in the Arctic area in the CMIP2 experiments. *SWECLIM Newsletter* **11**, 23–28.

Rind, D., deMenocal, P., Russell, G., Sheth, S., Collins, D. et al 2001. Effects of glacial meltwater in the GISS coupled atmosphere–ocean model 1. North Atlantic Deep Water response. *J. Geophys. Res.* **16**, 27 335–27 353.

Rühlemann, C., Mulitza, S., Müller, P. J., Wefer, G. and Zahn, R. 1999. Warming of the tropical Atlantic Ocean and slowdown of thermohaline circulation during the last deglaciation. *Nature* **402**, 511–514.

Schiller, A., Mikolajewicz, U. and Voss, R. 1997. The stability of the North Atlantic thermohaline circulation in a coupled ocean-atmosphere general circulation model. *Climate Dyn.* **13**, 325–347.

Simonsen, K. 1996. *Heat Budgets and Freshwater Forcing of the Nordic Seas and the Artic Ocean*. PhD Thesis. Nansen Environmental and Remote Sensing Center, Bergen, Norway.

Simonsen, K. and Haugan, P. M. 1996. Heat budgets of the Arctic Mediterranean and sea surface heat flux parametrizations for the Nordic Seas. *J. Geophys. Res.* **101**, 6553–6576.

Stommel, H. 1961. Thermohaline convection with two stable regimes of flow. *Tellus* **13**, 224–230.

Terray, L., Thual, O., Belamari, S., Déque, M., Dandin, P. et al 1995. Climatology and interannual variability simulated by the ARPEGE-OPA coupled model. *Climate Dyn.* **11**, 487–505.

Vellinga, M., Wood, R. A. and Gregory, J. M. 2002. Processes governing the recovery of a perturbed thermohaline circulation in HadCM3. *J. Climate* **15**, 764–780.

Visbeck, M., Chassignet, E. P., Curry, R., Delworth, T., Dickson, B. et al 2003. The ocean's response to North Atlantic Oscillation variability. In: *The North Atlantic Oscillation. Climatic significance and environmental impact* (eds J. W. Hurrell, Y. Kushnir, G. Ottersen, and M. Visbeck). *Geophysical Monograph 134*, American Geophysical Union, College Station, Washington DC, 113–146.

Welander, P. 1986. Thermohaline effects in the ocean circulation and related simple models. In: *Large-scale transport processes in the oceans and atmosphere* (eds J. Willebrand, and D. L. T. Anderson). Reidel, Dordrecht, 163–200.